ECS Transactions, 50 (40) 1-14 (2013)
10.1149/05040.0001ecst ©The Electrochemical Society

Synthesis and Electrochemical Properties of Ni Doped Spinel $LiNi_xMn_{2-x}O_4$ ($0 \leq x \leq 0.5$) Cathode Materials for Li-Ion Battery

Mesfin Kebede, Niki Kunjuzwa, Kenneth Ozoemena and Mkhulu Mathe

Energy Materials, Materials Science and Manufacturing, Council for Scientific and Industrial Research, P.O. Box 395, Pretoria, South Africa

Spherical pristine $LiMn_2O_4$ and Ni doped $LiNi_xMn_{2-x}O_4$ (x=0.1, 0.2, 0.3, 0.4, 0.5) cathode materials for lithium ion battery with high first cycle discharge capacity and excellent cycle performance were synthesized using the solution-combustion technique. XRD analysis revealed peak shift towards higher angle and lattice shrink as a result of Ni doping. CSAFM result confirms $LiNi_{0.5}Mn_{1.5}O_4$ provides higher current of 10nA than pristine $LiMn_2O_4$ of 0.05nA. The EIS result displays that small Ni content (x=0.1, 0.2) doping reduced the impedances of pristine $LiMn_2O_4$. The composition $LiNi_{0.1}Mn_{1.9}O_4$ exhibits higher capacity and better cycleability than other Ni content compositions. Charge/discharge cycling result shows that Ni substitution substantially improved the capacity retention of $LiMn_2O_4$. All Ni doped $LiNi_xMn_{2-x}O_4$ (x= 0.1, 0.2, 0.3, 0.4, 0.5) compositions are able to retain 99% of their respective first cycle discharge capacities, whereas $LiMn_2O_4$ retains only 60% of its first cycle discharge capacity of 122 mAh/g after 50 cycles.

Introduction

The development of cathode materials for lithium batteries that provide practical capacity, high voltage and long cycle life becomes so significant to meet the demands for high-power applications such as hybrid electric vehicles and power tools. $LiMn_2O_4$ spinel being one of the most promising positive (cathode) materials attracted the interest of researchers, due to its low cost, environmental friendliness and good safety (1, 2). However, the problem with spinel $LiMn_2O_4$ cathode material is it suffers severe capacity loss upon repeated charge/discharge cycling at elevated temperature. Some of the causes for capacity fading might be related with Mn dissolution in acidic electrolytes (3), Jahn-Teller distortion of Mn^{3+} at deeply discharge state (1), and oxygen deficiency (4). In order to tackle this problem, several research groups have synthesized cation substituted spinel materials $LiM_xMn_{2-x}O_4$ such as (M= Ni, Al, Fe, Co) with an intension of getting high-voltage plateaus as well as enhancing the cyclability. The compound $LiNi_{0.5}Mn_{1.5}O_4$ with a cubic spinel structure has been characterized as a high-voltage around 4.9V cathode material for lithium ion batteries (5, 6). Similarly $LiNi_{0.1}Mn_{1.9}O_4$ spinel cathode material was reported as Ni doped material with high cyclability (7).

The electrochemical performance of cathode materials varies with the synthesis methods. Specially, homogeneous dispersion of the cation substituting element in crystal lattice is so crucial in the synthesis of doped $LiM_xMn_{2-x}O_4$ (M = doping cation) cathode

materials. Generally solution synthesis techniques are preferable in order to get the required homogeneously doped composition without impurity unlike solid state reaction. Several solution synthesis methods of cation doped $LiMn_2O_4$ spinel structure have been reported, such as a spray-drying method (8), emulsion-drying method (9), molten salt method (10), sol-gel method (11). However, most of these methods involve complicated treatment processes or expensive reagents, which are time consuming and high cost for commercial applications. In this work, we have followed a simple and time efficient solution technique to synthesize spherical like pristine $LiMn_2O_4$ and Ni doped spinel structure $LiNi_xMn_{2-x}O_4$ (x=0.1, 0.2, 0.3, 0.4, 0.5) cathode materials by combustion method using urea as reducer and fuel. In addition we have scrutinized the effect of Ni content change on the structural, cell voltage, impedance and the discharge capacity stability of the spinel $LiNi_xMn_{2-x}O_4$ cathode material.

Experimental

Materials and chemicals

Synthesis of spherical $LiNi_xMn_{2-x}O_4$ spinels. The pristine $LiMn_2O_4$ and Ni-doped $LiNi_xMn_{2-x}O_4$ (x=0.1, 0.2, 0.3, 0.4, 0.5) spinel cathode materials with spherical morphology were synthesized by the solution combustion method wherein stoichiometric amounts of the precursors 99.9% pure $Li(NO_3)$, $Mn(NO_3)_2 \cdot 4H_2O$, $Ni(NO_3)_2 \cdot 4H_2O$ and CH_4N_2O were purchased from Sigma Aldrich and used as received without any further purification. The procedure used to prepare $LiMn_2O_4$ and $LiNi_xMn_{2-x}O_4$ (x=0.1, 0.2, 0.3, 0.4, 0.5) had the following stages. Appropriate mole ratios of Li, Mn and Ni nitrate salts and urea were dissolved and mixed in deionised water and stirred at ambient temperature for about 30 min to obtain homogeneously mixed solution. After that, the precursor solution was introduced into a furnace preheated at 500°C and then black powders were obtained. To investigate the effect of Ni ion content on the structural and electrochemical properties of $LiMn_2O_4$ cathode materials, pristine $LiMn_2O_4$ and doped samples with Ni ion concentration of 0.1, 0.2, 0.3, 0.4 and 0.5 were prepared under atmospheric pressure and then annealed at 700°C in air for 10hrs. The voluminous and foamy combustion ash was easily milled to obtain the final $LiMn_2O_4$ and $LiNi_xMn_{2-x}O_4$ (x=0.1, 0.2, 0.3, 0.4, 0.5) cathode materials.

Equipment and procedures

The morphology and energy-dispersive x-ray spectroscopy analysis (EDS) of the annealed samples $LiNi_xMn_{2-x}O_4$ were obtained using a high resolution scanning electron microscope (JEOL, JSM-7600F), operated at an accelerating voltage of 5 kV.

The structural properties of the samples were investigated by X-ray diffraction analysis using a PANalytical X'Pert PRO PW3040/60 X-ray diffractometer with Fe filtered Co- Kα (λ= 0.179026 nm) monochromated radiation source. Data were collected in the 2θ range of 10 – 90° at a scan rate of 2°/min.

The AFM topography images of the coated cathode materials were analysed using Agilent 5500 AFM (Agilent Technologies, USA). The current sensing images were obtained in the contact mode (CSAFM) with their corresponding topography images at a scanning rate of 0.5 Hz. For these images, a platinum coated (to allow conductivity) silicon probe with a force constant of 0.35 N/m was used. The bias voltage between the

samples and the tip, which creates the current which is used to construct a conductivity map, was set at 1 V. All the images were analyzed by the imaging processing software by Agilent, Pico Image version 6.2.

Electrochemical properties

Electrochemical cells were configured in the following way; coin cells of 2032 were assembled using lithium metal as anode, Celgard 2400 as separator, 1M solution of $LiPF_6$ in 50:50 (v/v) mixture of ethylene carbonate (EC) and diethylene carbonate (DEC) as the electrolyte. The cathode was made through a slurry coating procedure from a mix containing active material powder, conducting black and poly(vinylidene fluoride) binder in N-methyl-2-pyrrolidone in the proportion 80:10:10, respectively. The slurry was coated over aluminium foil and dried at 120°C over night for 12h. 18mm diameter slurry-coated aluminium foils electrodes were punched out and used as cathode. Coin cells were assembled in an argon filled glove box (MBraun, Germany) with moisture and oxygen levels maintained at less than 1 ppm. The cells were cycled at 30°C at 0.1C rate with respect to their corresponding theoretical capacities of $LiMn_2O_4$ and $LiNi_xMn_{2-x}O_4$ (x=0.1, 0.2, 0.3, 0.4, 0.5) using a MTI multi-channel battery tester. Electrochemical impedance spectroscopy (EIS) were conducted in a frequency range between 100 kHz and 10 mHz using an Autolab potentiostat PGSTAT 302N (Eco Chemie, Utrecht, Netherlands).

Results and discussion

Fig. 1a-f shows SEM images of $LiMn_2O_4$, $LiNi_{0.1}Mn_{1.9}O_4$, $LiNi_{0.2}Mn_{1.8}O_4$, $LiNi_{0.3}Mn_{1.7}O_4$, $LiNi_{0.4}Mn_{1.6}O_4$ and $LiNi_{0.5}Mn_{1.5}O_4$ samples, respectively. The SEM images display that the synthesized spinel $LiNi_xMn_{2-x}O_4$ (x=0, 0.1, 0.2, 0.3, 0.4, 0.5) cathode materials have spherical or spherical-like morphology with particle size of micrometers. Generally, spinel $LiMn_2O_4$ cathode materials with spherical morphology showed zero stress deviation on structures during charge/discharge reaction because the Jahn Teller distortions from a certain side can be counteracted by the opposite side of the spherical particles (12). The formation of microsized spherical particles is able to enhance the cycle life time of all the as-synthesized cathode materials including the pristine $LiMn_2O_4$ which will be discussed later under the results of Fig. 8.

Energy dispersive X-ray spectroscopy (EDS) elemental analysis was carried out in order to confirm successful doping of Ni ions. Though EDS cannot identify Li ion because of its small atomic size, it helped us to evaluate the Ni ion doping in the $LiMn_2O_4$ spinel cathode material. Fig. 2 displays the EDS elemental spectra of the samples. The EDS spectrum confirms that pristine $LiMn_2O_4$ and Ni doped $LiNi_xMn_{2-x}O_4$ spinel cathode materials were successfully synthesized using solution combustion techniques. The intensity of Ni peak increases as Ni content increases, which confirms the efficient doping of cations using this synthesis technique. The EDS quantitative elemental analysis of the samples has been given by table I. The atomic and weight percent of Ni increased with increase of doping Ni content, for the undoped sample the Ni content is zero. The carbon peak intensity value is from the carbon tape used to prepare the SEM samples.

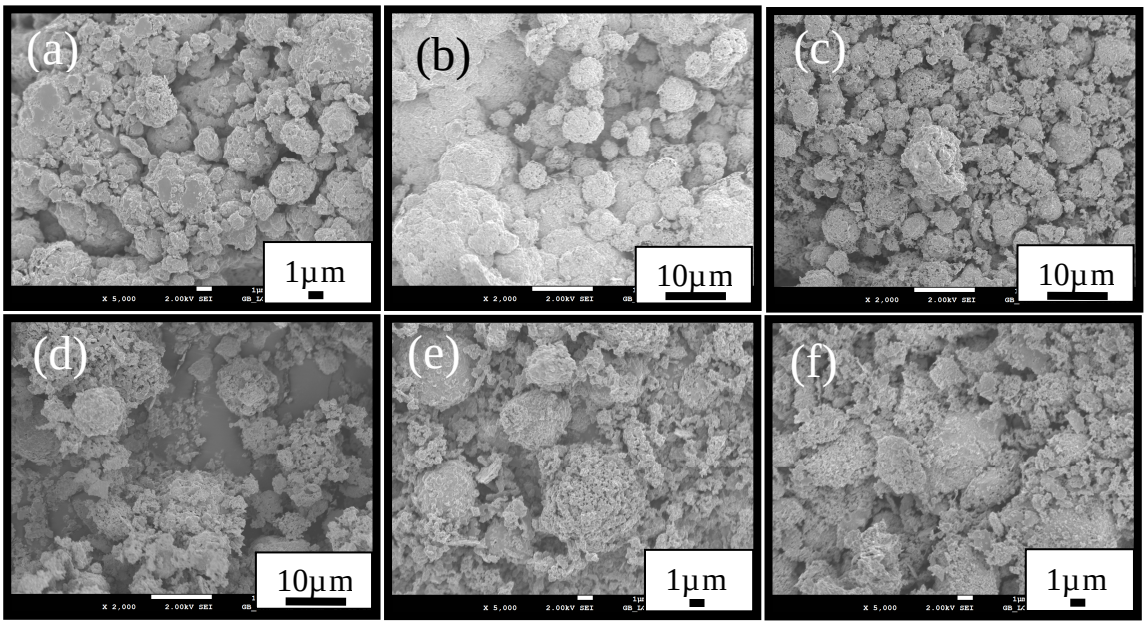

Figure 1. Top-view SEM micrographs of the products (a) $LiMn_2O_4$ (b) $LiNi_{0.1}Mn_{1.9}O_4$ (c) $LiNi_{0.2}Mn_{1.8}O_4$ (d) $LiNi_{0.3}Mn_{1.7}O_4$ (e) $LiNi_{0.4}Mn_{1.6}O_4$ and (f) $LiNi_{0.5}Mn_{1.5}O_4$.

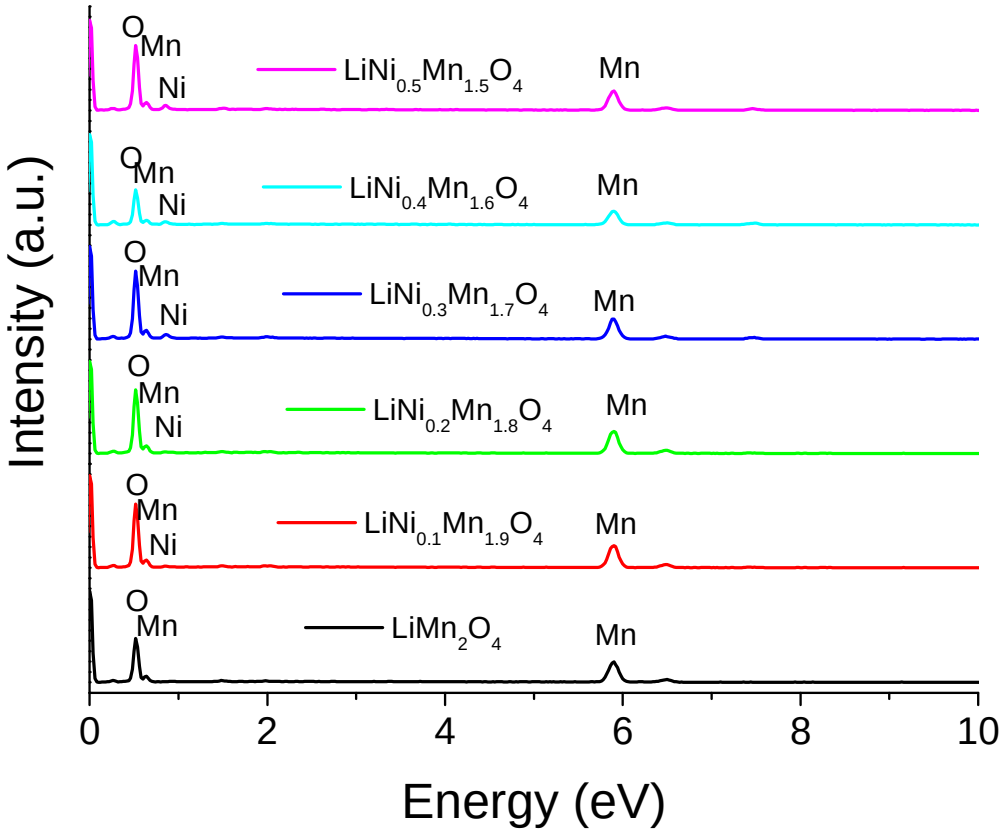

Figure 2. Energy dispersive X-ray spectroscopy result of synthesized $LiNi_xMn_{2-x}O_4$ (x=0, 0.1, 0.2, 0.3, 0.4, 0.5) cathode materials.

TABLE I. The elemental quantities of the samples obtained using EDS.

Sample composition	Element	Weight%	Atomic%
$LiMn_2O_4$	C K	3.90	9.10
	O K	33.79	59.15
	Mn K	62.31	31.76
$LiNi_{0.1}Mn_{1.9}O_4$	C K	3.76	8.38
	O K	37.78	63.22
	Mn K	55.75	27.16
	Ni K	2.71	1.24
$LiNi_{0.3}Mn_{1.7}O_4$	C K	4.12	8.85
	O K	40.54	65.39
	Mn K	47.48	22.30
	Ni K	7.86	3.46
$LiNi_{0.5}Mn_{1.5}O_4$	C K	3.43	7.50
	O K	40.15	65.82
	Mn K	48.34	23.08
	Ni K	8.07	3.61

Fig. 3(a) represents a typical X-ray diffraction pattern of as-synthesized samples. The examination of the diffraction patterns confirms that all recognizable reflection peaks including (111), (311), (222), (400), (331), (511) and (440) can be clearly indexed to the single phase of the spinel cubic structure of $LiMn_2O_4$ (JCPDS File No. 88-1749) with space group Fd3m and with out any impurity peaks. There is no significant difference in the crystal structure after the doping. This indicates that the Ni^{2+} dopant ions have placed at Mn^{3+} site in $LiMn_2O_4$ and no other phase is formed. All the peaks are very sharp, indicating a high crystallinity of the powders. However, by zooming in (111) plane as shown in Fig. 3(b), it is seen that the Bragg diffraction peaks go to the higher angle slightly with the increase in the amount of nickel doped. The diffraction peaks noticeably shift to higher angles and the lattice parameter decreases with the substitution of Ni^{2+} for Mn^{3+} which reveals that the crystal structure is shrunken with Ni^{2+} content in the doped $LiMn_2O_4$ phase. This decrease of lattice parameter is due to the increase in the concentration of small Mn^{4+}(0.53Å) ions in the spinel structure as large Mn^{3+}(0.645Å) ions are substituted by Ni^{2+}(0.69Å) ions in the samples $LiNi_xMn_{2-x}O_4$ (x=0.1, 0.2, 0.3, 0.4, 0.5).

The variation in lattice parameter and the corresponding unit cell volume of the samples as a result of Ni doping is summarized using Table II. The lattice parameter of the as-synthesized pristine $LiMn_2O_4$ is calculated to be 8.224 Å. When the spinel $LiMn_2O_4$ cathode material is doped with Ni, the lattice parameter of the doped $LiNi_xMn_{2-x}O_4$ (x=0.1, 0.2, 0.3, 0.4, 0.5) cathode materials exhibiting a trend of decrease in lattice parameter up to 8.127 Å when the Ni content becomes x=0.5. Consequently the unit cell volume reduces almost by 20 $Å^3$ as the Ni doping content reaches x=0.5. We have observed the effect of Ni doping content in stabilizing the spinel $LiMn_2O_4$ crystal structure during charge/discharge cycling. All the Ni doped samples are able to retain about 99% of the first cycle discharge capacity after 50 cycles. On the other hand, the first cycle discharge capacity keep on decreasing proportionally with increase in doping Ni content as it is expected (8).

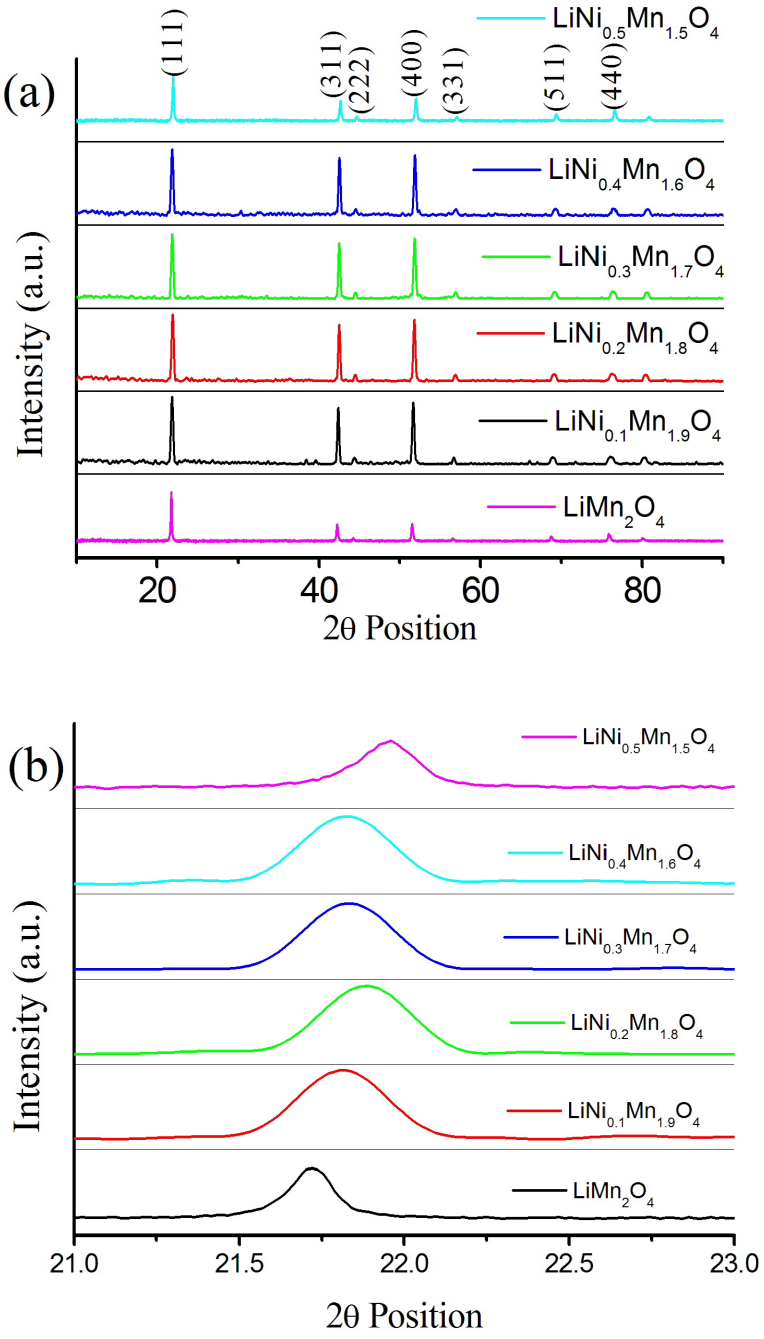

Figure 3. (a) X-ray diffraction pattern and (b) diffraction peak shift for (111) plane of synthesized $LiNi_xMn_{2-x}O_4$ (x=0, 0.1, 0.2, 0.3, 0.4, 0.5) spinel cathode materials.

Table II. Structural parameters obtained from Rietveld Refinement of LiNixMn2-xO4 (x=0, 0.1, 0.2, 0.3, 0.4, 0.5) samples.

	a (Å)	**Unit cell volume (Å^3)**
$LiMn_2O_4$	8.224	556.223
$LiNi_{0.1}Mn_{1.9}O_4$	8.188	548.950
$LiNi_{0.2}Mn_{1.8}O_4$	8.161	543.538
$LiNi_{0.3}Mn_{1.7}O_4$	8.180	547.343
$LiNi_{0.4}Mn_{1.6}O_4$	8.182	547.745
$LiNi_{0.5}Mn_{1.5}O_4$	8.127	536.773

Furthermore, we have examined the arrangement of Ni ions within the lattice of selected $LiNi_{0.5}Mn_{1.5}O_4$ sample using FT-IR spectroscopy. As it has been reported, that $LiNi_{0.5}Mn_{1.5}O_4$ has two different space groups, Fd3m or $P4_332$ depending on Ni ordering in the lattice (10). X-ray diffraction analysis is unable to distinguish between these two space groups because of the similar scattering factors of Ni and Mn. As it is shown using the FT-IR spectrum in Fig. 4, sample $LiNi_{0.5}Mn_{1.5}O_4$ has two bands at 621 cm^{-1} which are more intensive than those at 580 cm^{-1}. Such a special feature indicates a disordered structure of space group of *Fd*3*m* (13). In addition, two bands which are supposed to occur at 650 cm^{-1} for *P*4_332 phase were absent or undefined in our spectrum, which further proves a disordering distribution of Ni in the structure of as-synthesized $LiNi_{0.5}Mn_{1.5}O_4$.

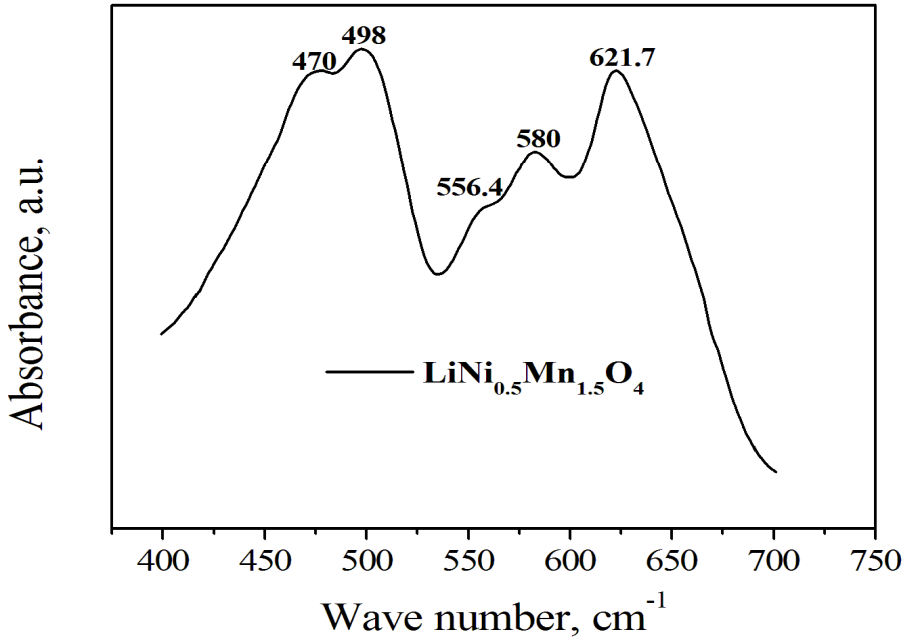

Figure 4. The FT-IR absorption spectrum of $LiNi_{0.5}Mn_{1.5}O_4$ sample.

To analyze the electrochemical performance of the as-synthesized cathode materials, first we have calculated their theoretical capacity, C_T, using the well-known expression (14):

$$C_T = 26.8\, p/M \qquad [1]$$

where *p* and *M* denote the number of Mn(III) and the molecular weight of ion-doped $LiMn_2O_4$, respectively. Employing equ.1, the theoretical capacity of $LiMn_2O_4$, $LiNi_{0.1}Mn_{1.9}O_4$, $LiNi_{0.2}Mn_{1.8}O_4$, $LiNi_{0.3}Mn_{1.7}O_4$, $LiNi_{0.4}Mn_{1.6}O_4$ and $LiNi_{0.5}Mn_{1.5}O_4$ is found to be 148 mAh/g, 147.9 mAh/g, 147.6 mAh/g, 147.3 mAh/g, 147.0 mAh/g and 146.6 mAh/g, respectively. Charge/discharge capacity performance of the cathode materials carried out at 0.1C rates with respect to their corresponding theoretical capacities.

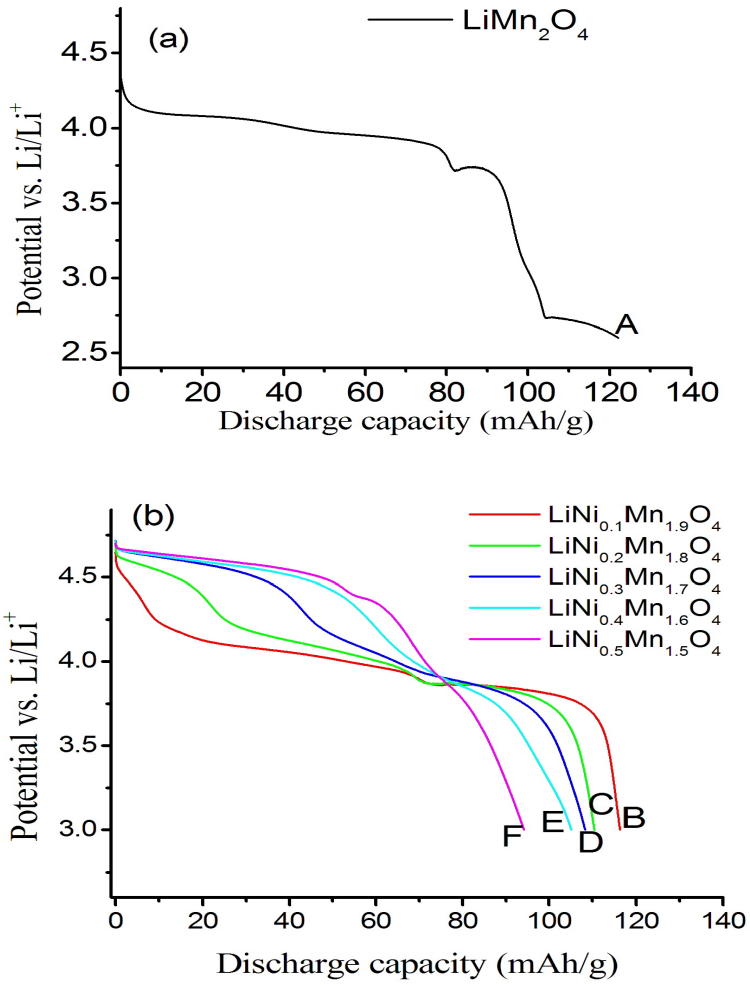

Figure 5. First cycle discharge capacity of (a) pristine $LiMn_2O_4$ and (b) $LiNi_xMn_{2-x}O_4$ (x= 0.1, 0.2, 0.3, 0.4, 0.5) spinel cathode materials.

The representative first cycle discharge capacities of $LiMn_2O_4$, $LiNi_{0.1}Mn_{1.9}O_4$, $LiNi_{0.2}Mn_{1.8}O_4$, $LiNi_{0.3}Mn_{1.7}O_4$, $LiNi_{0.4}Mn_{1.6}O_4$ and $LiNi_{0.5}Mn_{1.5}O_4$ are displayed by the curves **A**, **B**, **C, D, E and F** in Fig. 5(a) and (b), respectively. During the first cycle pristine spinel $LiMn_2O_4$ delivered discharge capacity of around 122 mAh/g and plateau at 3.49V. As it can be seen in curve **B, C, D, E and F**, $LiNi_xMn_{2-x}O_4$ (x=0.1, 0.2, 0.3, 0.4, 0.5) when Ni content increases the sample first discharge capacity found to be 116.4 mAh/g, 110.5 mAh/g, 108.3 mAh/g, 105.1 mAh/g, 95.5 mAh/g and provide mean cell voltage of 4.0 V, 4.11 V, 4.18 V, 4.57 V, 4.6 V respectively. For Ni doped sample curves for instance $LiNi_{0.5}Mn_{1.5}O_4$ has two plateaus at around 4.6 V and 3.8 V due to the Ni^{2+}/Ni^{4+} redox and Mn^{3+}/Mn^{4+} redox couple, respectively (15). The first cycle discharge capacity delivered and corresponding mean voltage values for the synthesized samples is summarized in table III. The discharge capacities of the as-synthesized cathode materials are comparable to what experimentally reported values (7). All the cathode samples prepared are well performing materials. It is noteworthy that the cell potential has increased from 3.49 V of $LiMn_2O_4$ to 4.6 V for $LiNi_{0.5}Mn_{1.5}O_4$ and thus the doped materials can be considered as high voltage cathode materials. One can have the option to make selection of the doping Ni content based on the desired discharge capacity and

voltage delivered by the samples. The specific capacity of the samples decreases with the increase in the amount of Ni substitution. This phenomenon can be explained as, the reversibly extractable Li^+ ions amount decreases from "1" for pristine $LiMn_2O_4$ to "1-x" for Ni substituted lithium manganese oxides upon substitution of electrochemically active Mn^{3+} ions (8).

Table III. First cycle discharge capacities delivered and mean voltage by the synthesized samples.

Sample composition	1st discharge capacity (mAh/g)	Voltage (V)
$LiMn_2O_4$	122	3.49
$LiNi_{0.1}Mn_{1.9}O_4$	116.4	4.00
$LiNi_{0.2}Mn_{1.8}O_4$	110.5	4.11
$LiNi_{0.3}Mn_{1.7}O_4$	108.3	4.18
$LiNi_{0.4}Mn_{1.6}O_4$	105.1	4.57
$LiNi_{0.5}Mn_{1.5}O_4$	95.5	4.60

We employed a current sensor atomic force microscopy (CSAFM) which is a reliable technique to study the electrical conductivity of the active materials of cathode materials. CSAFM measurements showed that the average conductance increased significantly with increased Ni doping content.

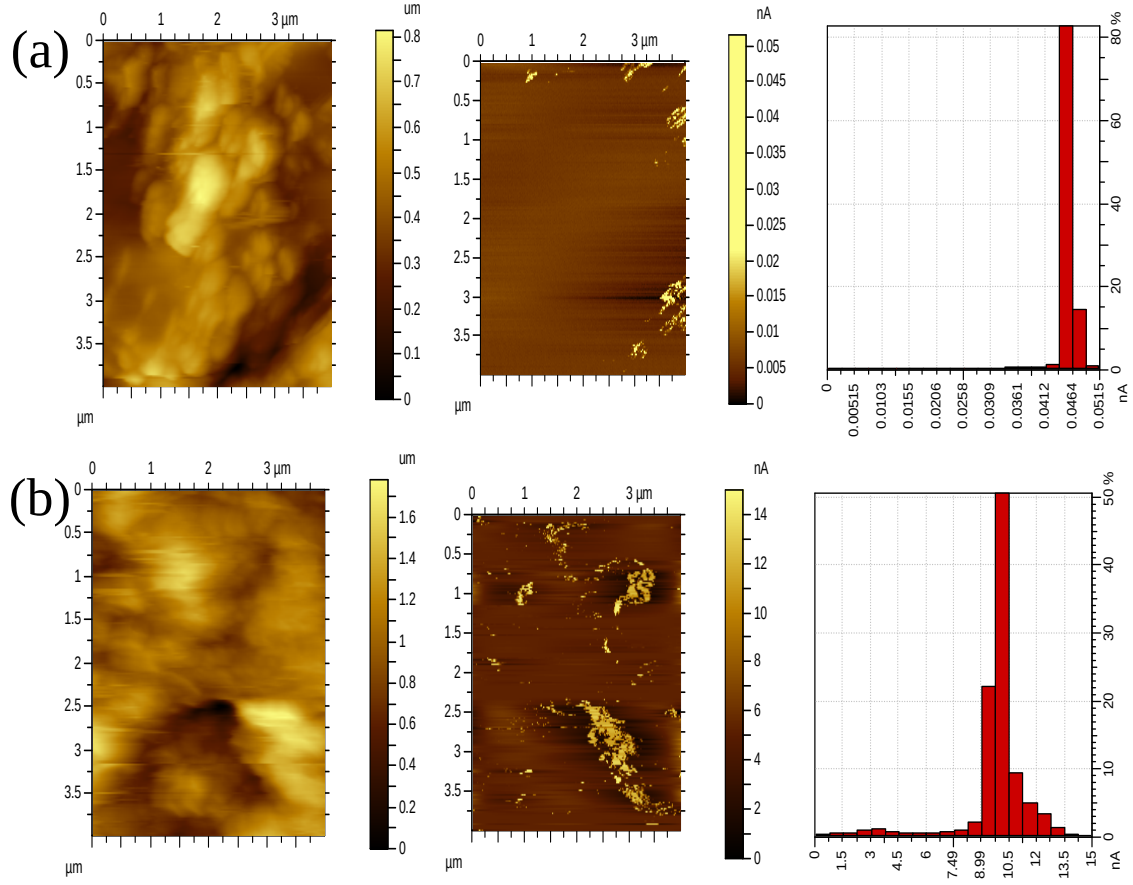

Figure 6. The CSAFM image and current distribution profile for (a) $LiMn_2O_4$ and (b) $LiNi_{0.5}Mn_{1.5}O_4$ samples, respectively.

The AFM topography and conductance images of the coated $LiMn_2O_4$ and $LiNi_{0.5}Mn_{1.5}O_4$ cathode materials are shown respectively in Fig. 6(a) and (b). The histogram in Fig. 6(a) and (b) shows the CSAFM results indicating a current conductivity profile for the pristine $LiMn_2O_4$ and Ni doped $LiNi_{0.5}Mn_{1.5}O_4$ samples, respectively. And it is seen that there is higher current in the doped sample going up to 10 nA compared to the pristine which has only 0.05 nA. The electrical current data extracted from the current map indicates that the $LiNi_{0.5}Mn_{1.5}O_4$ sample shows reading that is significantly higher than the pristine $LiMn_2O_4$. The Ni doped sample shows that 85% of the values fall between 9 and 12 nA while the other 15% are distributed from 0 to 15 nA. However, the total electrical current values of the pristine $LiMn_2O_4$ cathode material fall between 0.04 and 0.06 nA. We assume that this high surface current contributed towards enhancing the cycleability of the doped samples.

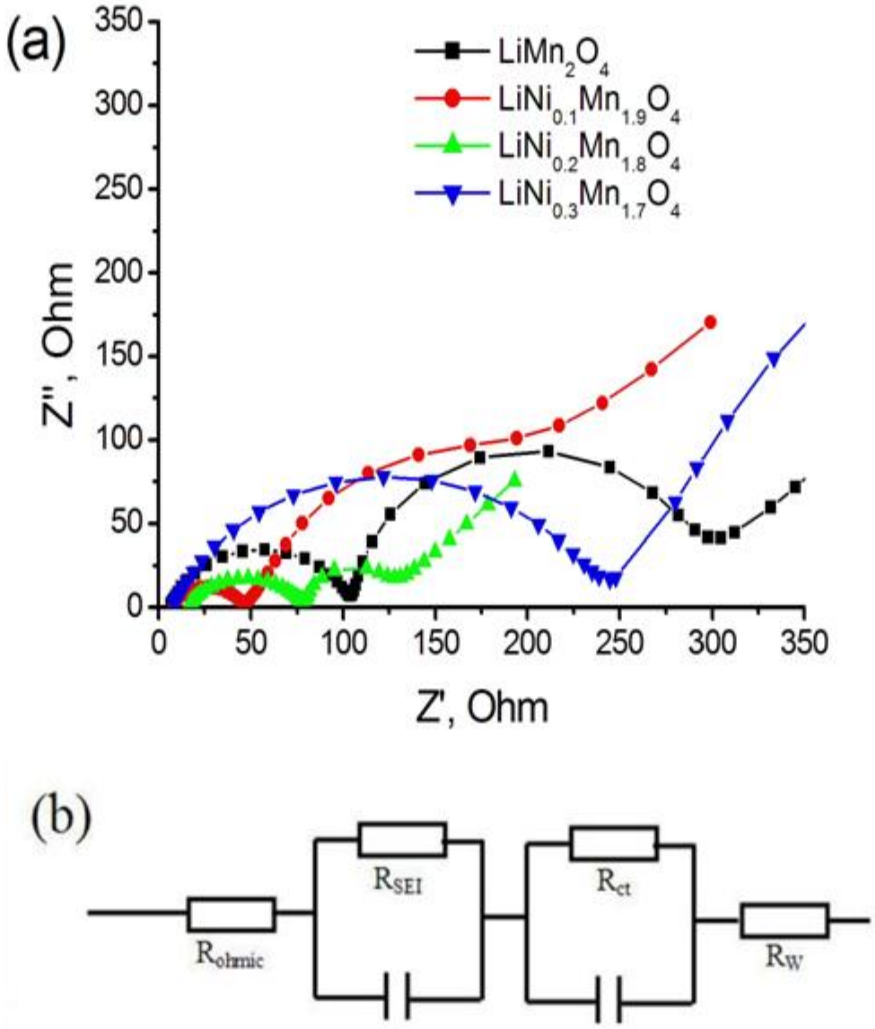

Figure 7. (a) EIS results of $LiNi_xMn_{2-x}O_4$ (x= 0, 0.1, 0.2, 0.3) samples and (b) corresponding equivalent circuit.

In order to understand better the effect of doping Ni ion on the impedance of spinel $LiMn_2O_4$, we carried out AC impendence studies of the cells of pristine $LiMn_2O_4$, $LiNi_{0.1}Mn_{1.9}O_4$, $LiNi_{0.2}Mn_{1.8}O_4$ and $LiNi_{0.3}Mn_{1.7}O_4$. Fig. 7(a) shows the EIS plots obtained for $LiMn_2O_4$, $LiNi_{0.1}Mn_{1.9}O_4$, $LiNi_{0.2}Mn_{1.8}O_4$ and $LiNi_{0.3}Mn_{1.7}O_4$. These Nyquist plots were fitted using the equivalent circuit shown in Fig. 7(b) and the fitting impedance parameters are reported in Table IV. The Ni doping has shown significant impact in decreasing the R_{SEI} and R_{ct} impedances. The result indicates that small content of nickel x=0.1 and x=0.2 decreases the impedance. Beyond x=0.3 the impedance starts to increase. This result shows that small Ni content is preferred to get better performance.

Table IV. The EIS parameters for synthesized $LiNi_xMn_{2-x}O_4$ (x=0, 0.1, 0.2, 0.3) cathode materials.

Ni_x	$R_{ohmic}(\Omega)$	R_{SEI} (Ω)	R_{ct} (Ω)	a (Å)
0.0	6.1	170.8	98.6	8.224
0.1	7.2	90.3	38.3	8.188
0.2	15.3	38.8	63.6	8.161
0.3	7.7	303.6	231.6	8.180

R_{ohmic} represents the solution resistance; R_{SEI} signify the diffusion resistance of Li^+ ions through the solid-electrolyte interface (SEI) layer; R_{ct} corresponds to the charge transfer resistance (16).

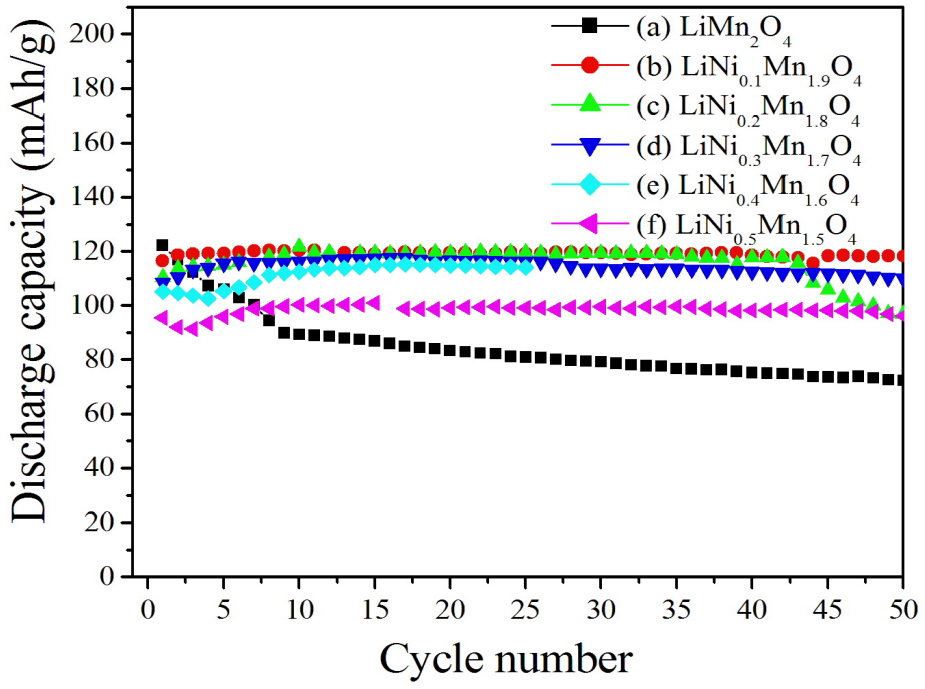

Figure 8. The discharge capacity vs. cycle number for LiNixMn2-xO4 (a) x=0, (b) x=0.1, (c) x=0.2, (d) x=0.3, (e) x=0.4, and (f) x=0.5 samples

To compare and examine the battery performance of synthesized pristine and Ni doped spinel cathode materials, 50 charge/discharge cycles of a lithium battery employing $LiMn_2O_4$, $LiNi_{0.1}Mn_{1.9}O_4$, $LiNi_{0.2}Mn_{1.8}O_4$, $LiNi_{0.3}Mn_{1.7}O_4$, $LiNi_{0.4}Mn_{1.6}O_4$ and $LiNi_{0.5}Mn_{1.5}O_4$ cathode were performed at a constant current of 0.1C rate. Fig. 8 curve (a) is obtained from the pristine $LiMn_2O_4$ and it retained only 60% of its first cycle discharge capacity of 122mAh/g. Fig. 8 curve (b), (c), (d), (e) and curve (f) respectively represents cyclic performance of $LiNi_{0.1}Mn_{1.9}O_4$, $LiNi_{0.2}Mn_{1.8}O_4$, $LiNi_{0.3}Mn_{1.7}O_4$, $LiNi_{0.4}Mn_{1.6}O_4$ and $LiNi_{0.5}Mn_{1.5}O_4$. All Ni ion substituted samples $LiNi_xMn_{2-x}O_4$ (x=0.1, 0.2, 0.3, 0.4, 0.5) exhibited a very good cycleability, they retained 99% of their respective first cycle discharge capacity after 50 cycles, however the first cycle discharge capacity of Ni doped decreases with Ni content. The capacity retention of the Ni substituted spinels is significantly enhanced in comparison with that of $LiMn_2O_4$. The possible reasons for the observed behavior are, first there may be a considerable decrease in the effect of Jahn-Teller distortion when substituting a small amount of Ni for Mn in the spinel. Second, there may be a reduction in spinel dissolution.

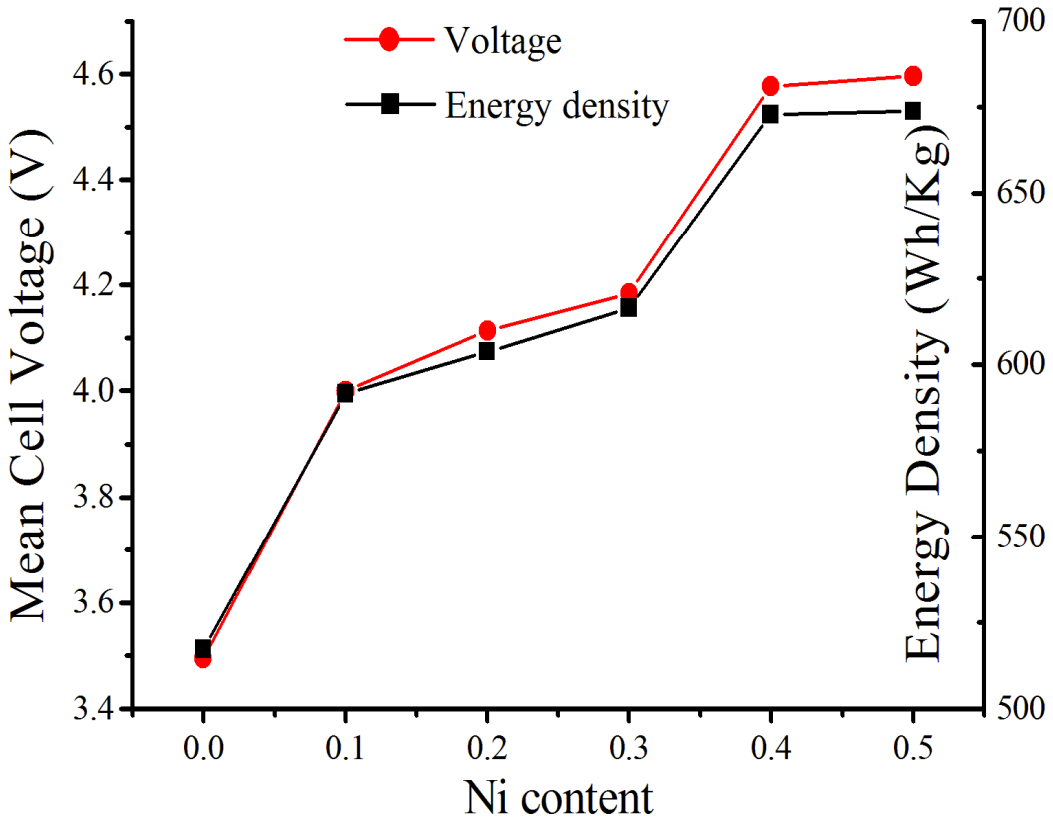

Figure 9. Represents the mean cell voltage and cell energy density vs the Ni content of the samples $LiNi_xMn_{2-x}O_4$ (x=0, 0.1, 0.2, 0.3, 0.4, 0.5).

It can be clearly seen in Fig. 9, the mean cell voltage increases almost linearly with increase in Ni content doping. The average cell voltage increases from 3.49 V of pristine $LiMn_2O_4$ up to 4.6 V of $LiNi_{0.5}Mn_{1.5}O_4$. The possible reasons that the synthesized Ni doped $LiNi_xMn_{2-x}O_4$ cathode materials deliver higher voltage compared to pristine $LiMn_2O_4$ are; the first one because of the low Fermi energy of Li^+ ion (17), the other

reason is Ni^{2+} ion has increased the electrical conductivity of the Ni doped materials. Furthermore, it can be noticed that the energy density of the synthesized cathode materials has increased from 510 Wh/Kg to 690 Wh/Kg as the Ni doping content increased linearly to 0.5.

Conclusion

In summary, we successfully synthesized spherical like pristine $LiMn_2O_4$ and Ni ion doped $LiNi_xMn_{2-x}O_4$ (x=0.1, 0.2, 0.3, 0.4, 0.5) cathode materials using solution combustion method for Li-ion batteries application. The samples were characterized by SEM, EDS, XRD, CSAFM, FTIR, EIS and battery charge/discharge testing. The morphology and particle size of the synthesized pristine and Ni doped $LiNi_xMn_{2-x}O_4$ samples is found to be spherical and micro sized. The spherical morphology appears to give better cycleability for all samples compared to what has been reported till now. The XRD result proved that the crystal structure of $LiMn_2O_4$ was contracted because of Ni doping. CSAFM confirmed that Ni doped $LiNi_{0.5}Mn_{1.5}O_4$ sample has high current of 10 nA compared to $LiMn_2O_4$ with low current of 0.05nA. The EIS result indicated that small Ni doped samples (x=0.1 and 0.2) have smaller solid-electrolyte interface and charge transfer impedances than pristine $LiMn_2O_4$ sample. All Ni ion substituted samples show high cycleability about 99% of their first cycle discharge capacity whereas $LiMn_2O_4$ retains 60% of its first cycle discharge capacity after 50 cycles. In addition, we have found that the sample $LiNi_{0.1}Mn_{1.9}O_4$ exhibited higher first cycle discharge capacity and better cycleability than the other samples which have more Ni ion content. The decrease in lattice parameter and high electrical conductivity of the doped samples as a result of Ni doping remarkably improved the cycling stability of $LiMn_2O_4$ spinel cathode material.

Acknowledgments

The financial support of this work from NRF and CSIR is highly acknowledged. The authors would like to acknowledge Charl Jafta for assisting in the acquisition of the CS-AFM data.

References

1. T. Ohzuku, M. Kitagawa and T. Hirai, *J.Electrochem.Soc.*, **137**, 3 (1990).

2. R. Gummow, A. De Kock and M. Thackeray, *Solid State Ionics.*, **69**, 1 (1994).

3. D. H. Jang, Y. J. Shin and S. M. Oh, *J.Electrochem.Soc.*, **143**, 7 (1996).

4. Y. Xia, T. Sakai, T. Fujieda, X. Yang, X. Sun, Z. Ma, J. McBreen and M. Yoshio, *J.Electrochem.Soc.*, **148**, 7 (2001).

5. K. Amine, H. Tukamoto, H. Yasuda and Y. Fujita, *J.Power Sources.*, **68**, 2 (1997).

6. R. Alcantara, M. Jaraba, P. Lavela and J. Tirado, *Electrochim.Acta.*, **47**, 11 (2002).

7. X. Gu, X. Li, L. Xu, H. Xu, J. Yang and Y. Qian, *Int.J.Electrochem.Sci.*, **7** (2012).

8. H. Wu, J. Tu, X. Chen, Y. Li, X. Zhao and G. Cao, *Journal of Solid State Electrochemistry.*, **11**, 2 (2007).

9. S. T. Myung, S. Komaba, N. Kumagai, H. Yashiro, H. T. Chung and T. H. Cho, *Electrochim.Acta.*, **47**, 15 (2002).

10. J. H. Kim, S. T. Myung, C. Yoon, S. Kang and Y. K. Sun, *Chemistry of materials.*, **16**, 5 (2004).

11. B. Hwang, Y. Wu, M. Venkateswarlu, M. Cheng and R. Santhanam, *J.Power Sources.*, **193**, 2 (2009).

12. H. L. Zhu, Z. Y. Chen, S. Ji and V. Linkov, *Solid State Ionics.*, **179**, 27 (2008).

13. M. Kunduraci, J. F. Al-Sharab and G. G. Amatucci, *Chemistry of materials.*, **18**, 15 (2006).

14. T. Kakuda, K. Uematsu, K. Toda and M. Sato, *J.Power Sources.*, **167**, 2 (2007).

15. Y. J. Lee, C. Eng and C. P. Grey, *J.Electrochem.Soc.*, **148**, 3 (2001).

16. J. Xie, X. Zhao, G. Cao, M. Zhao and S. Su, *J.Power Sources.*, **140**, 2 (2005).

17. P. G. Bruce, *CHEMICAL COMMUNICATIONS-CHEMICAL SOCIETY.*, (1997).